10 Particle Physics at DESY/HERA (H1)

K. Müller, P. Robmann, U. Straumann, and P. Truöl

in collaboration with C. Grab (Institut für Teilchenphysik der ETH, Zürich), S. Egli, M. Hildebrandt and R. Horisberger (Paul–Scherrer–Institut, Villigen), and 39 institutes outside Switzerland

(H1 - Collaboration)

As mentioned already in last years annual report the improved extraction of the parton-density functions (PDFs) remained a central topic of the recent publications based on the data collected until 2007 by the H1-collaboration at the HERA electron-proton storage ring. Statistical and systematic errors of both neutral and charged current cross sections as a function of Q^2 and Bjorken-x [4] have been reduced either by combining all available H1 data or by combining data from the H1 and ZEUS experiments.

The completion of the analysis of inclusive neutral (NC) and charged (CC) current cross sections with the HERA I and HERA II H1 data samples at $\sqrt{s} = 319$ GeV is documented in a long article [1] which is briefly reviewed below. The combination of the charm production data from the two experiments and their impact on the extraction of PDFs examplifies the second approach [2].

10.1 Neutral and charged current cross sections

For the measurement of the inclusive deep-inelastic scattering (DIS) cross sections [1] for $e^{\pm}$ interactions data from 333.7 pb^{-1} of integrated luminosity were available. The e^-p data correspond to an almost tenfold increase in luminosity over the HERA I data set. Moreover, the operation of the HERA collider with left and right handed longitudinally polarised electron and positron beams allowed measurements in the NC and CC channels with four distinct initial states. The cross sections cover the region $Q^2 \geq 100$ GeV^2 and Bjorken-$x \geq 10^{-3}$, and were obtained differentially in Q^2 and double-differentially in x and Q^2. In the NC channel a systematic uncertainty of 1.5% was attained in the kinematic region $Q^2 < 1000$ GeV^2 and $y > 0.1$ [5], compared to a statistical accuracy of 1 - 3 %. An important input leading to this higher precision stemmed from the new determination of the integrated luminosity using elastic QED Compton scattering $e^+p \rightarrow e^+p\gamma$ events [3]. The high inelasticity region of $0.63 \leq y \leq 0.90$ for $60 \leq Q^2 \leq 800$ GeV^2 was covered in the NC analy-

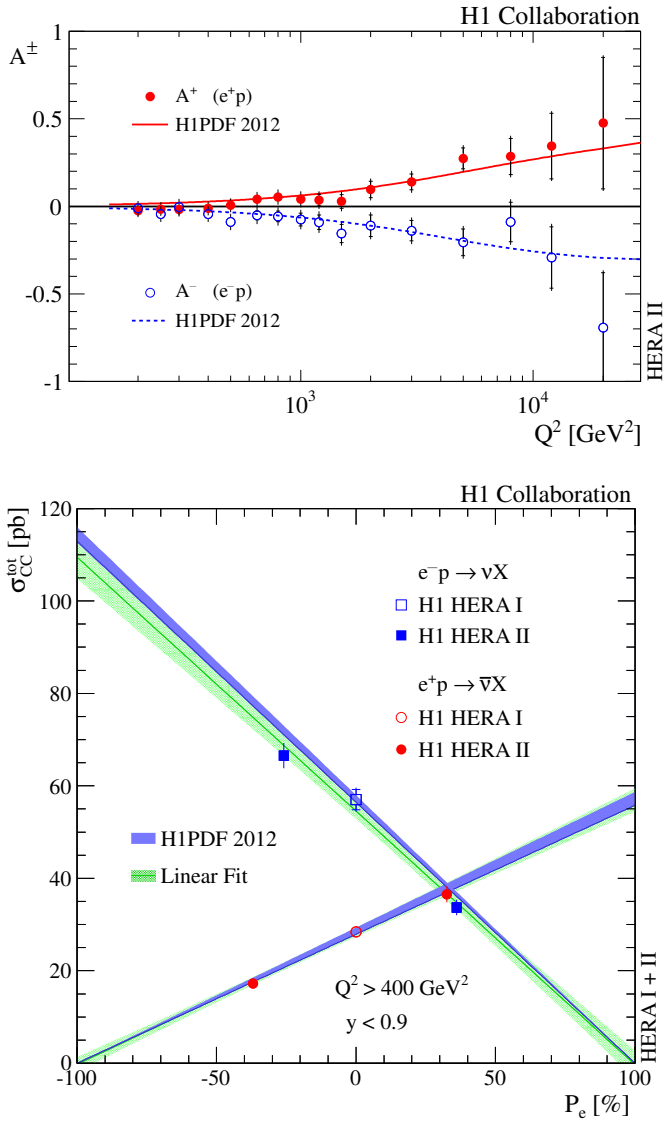

FIG. 10.1 – Top: Q^2 dependence of the polarisation asymmetries A^+ and A^- for e^+p and e^-p, respectively. Bottom: dependence of the $e^{\pm}p$ total CC cross sections on the lepton beam polarisation. In both plots the measurements are compared to the Standard Model expectation based on the H1PDF 2012 parametrisation. The green band (bottom) corresponds to the $\pm 1\sigma$ error of a linear fit. Inner and outer error bars represent the statistical and total errors, respectively.

[4] Q^2: square of the four-momentum exchanged in the hard $e^{\pm}$ scattering process,
x: longitudinal component of the incoming proton's momentum carried by the interacting parton (quark or gluon).
[5] inelasticity $y \equiv Q^2/x \cdot s$ with s: total centre-of-mass energy

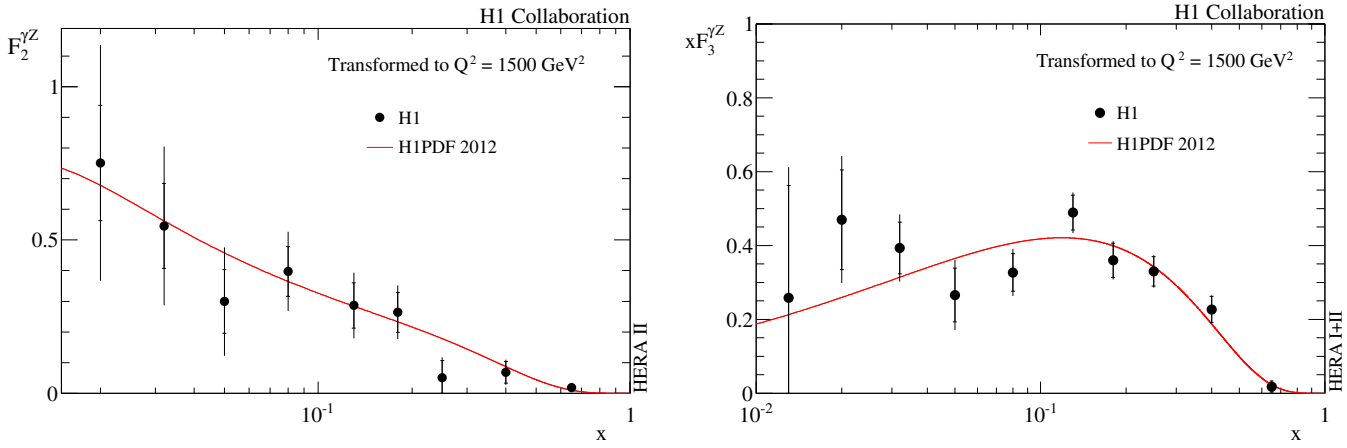

FIG. 10.2 –
Measured structure functions $F_2^{\gamma Z}$ and $xF_3^{\gamma Z}$ transformed to $Q^2 = 1500$ GeV^2 compared to the H1PDF 2012 predictions.

sis for unpolarised $e^{\pm}p$ scattering. This region of phase space is sensitive to the F_L structure function. The article includes the results of a next-to-leading order (NLO) QCD analysis for $Q^2 \geq 3.5$ GeV^2 including all previously published H1 NC and CC cross section measurements (H1PDF2012). The measurements are well described by the QCD fit over the full phase space (χ^2 per degree of freedom 1570/1461). The new results at high Q^2 provide better constraints on the PDFs. In particular the CC e^+p data enabled an improved flavour separation at high x. The NC lepton polarisation asymmetry $A^{\pm}$, sensitive to parity violation, was determined both for e^+p and e^-p scattering and found to increase with Q^2 in agreement with the expectation of the Standard Model (see Fig. 10.1).

The structure function $F_2^{\gamma Z}$ (which is associated with the photon-Z interference, see below for definition) was measured for the first time using the polarisation dependence of the $e^{\pm}p$ NC cross section. At high Q^2 the structure function $xF_3^{\gamma Z}$ is determined using unpolarised NC cross sections obtained from the complete HERA I and HERA II data sets. The $xF_3^{\gamma Z}$ results cover the range $0.013 \leq x \leq 0.65$. Integrated over x the measurement validates a sum rule for charged lepton scattering. Figure 10.2 shows the averaged results for both these structure functions at $Q^2 = 1500$ GeV^2.

The structure functions F_2 and F_3 appear in the general expression for the neutral current cross section:

$$\frac{d^2\sigma^{\pm}_{\rm NC}}{dx\,dQ^2} = \frac{2\alpha\pi^2}{xQ^4}\left(Y_+\tilde{F}_2^{\pm} \mp Y_- x\tilde{F}_3^{\pm} - y^2\tilde{F}_L^{\pm}\right)(1+\Delta^{\rm weak}_{\rm NC})$$

where $Y_{\pm}$ are kinematical functions and y is the lepton energy loss. The generalized structure functions, $\tilde{F}_{2,3}$ may be written as linear combinations of the proton structure functions F_2, $F_{2,3}^{\gamma Z}$ and $F_{2,3}^{Z}$ which contain information on the parton dynamics as well as on the electroweak couplings of the quarks to the neutral vector bosons. F_2 is associated to pure photon exchange terms, $F_{2,3}^{\gamma Z}$ to photon-Z interference and $F_{2,3}^{Z}$ to pure Z-exchange. $\tilde{F}_L$ may be decomposed similarly, but is important only at high y and negligible at large x and Q^2.

The sensitivity to the quark (antiquark) $q(\bar{q})$ distribution functions arises as

$$\begin{aligned}\left[F_2, F_2^{\gamma Z}, F_2^{Z}\right] &= x\sum_i \left[e_i^2, 2e_iv_i, v_i^2+a_i^2\right](q_i+\bar{q}_i)\\ \left[xF_3^{\gamma Z}, xF_3^{Z}\right] &= 2x\sum_i \left[e_ia_i, v_ia_i\right](q_i-\bar{q}_i)\end{aligned}$$

The linear combinations for $\tilde{F}_2$ and $x\tilde{F}_3$ for a lepton beam with polarisation P_e are given as

$$\begin{aligned}\tilde{F}_2^{\pm} &= F_2 - (v_e \pm P_e a_e)\kappa\lambda(Q^2)F_2^{\gamma Z} + \\ &\quad (a_e^2+v_e^2 \pm P_e 2v_e a_e)[\kappa\lambda(Q^2)]^2F_2^{Z}\\ x\tilde{F}_3^{\pm} &= -(a_e \pm P_e v_e)\kappa\lambda(Q^2)xF_3^{\gamma Z} + \\ &\quad (2a_ev_e \pm P_e[v_e^2+a_e^2])[\kappa\lambda(Q^2)]^2xF_3^{Z}\end{aligned}$$

with $\kappa^{-1} = 4(M_W/M_Z)^2[1-(M_W/M_Z)^2]$, $\lambda(Q^2) = Q^2/(Q^2+M_Z^2)$, and $a(v)$ designating the axialvector (vector) couplings of the quarks and leptons.

Similar expressions hold for the charged current cross section yielding a flavor decomposition:

$$\frac{d^2\sigma^{-}_{\rm CC}}{dx\,dQ^2} = (1\pm P_e)\frac{G_F^2}{4\pi x}\left[\frac{M_W^2}{M_W^2+Q^2}\right]^2\left(Y_+W_2^{\pm} \mp Y_- xW_3^{\pm} - y^2W_L^{\pm}\right)\cdot\left(1+\Delta^{\rm weak}_{\rm CC}\right)$$

with:

$$W_2^- = x(U+\overline{D}) \qquad W_2^+ = x(\overline{U}+D)$$
$$xW_3^- = x(U-\overline{D}) \qquad xW_3^- = x(-\overline{U}+D)$$
$$U = u+c \qquad \overline{U} = \overline{u}+\overline{c}$$
$$D = d+s \qquad \overline{D} = \overline{d}+\overline{s}.$$

The polarisation dependence of the CC total cross section for $Q^2 > 400$ GeV^2 and $y < 0.9$ was measured and compared to the unpolarised HERA I measurements. As evident from Fig. 10.1 the data exhibit a linear scaling of the cross sections with P_e which is positive for e^+p and negative for e^-p scattering. The data are consistent with the absence of right handed weak currents.

10.2 Open charm production

Measurements of open charm production in deep-inelastic ep scattering by the H1 and ZEUS experiments using different charm tagging methods were combined, accounting for the systematic correlations [2]. The measurements were extrapolated to the full phase space using a NLO QCD calculation to obtain the reduced charm quark-pair cross sections in the region of photon virtualities $2.5 \leq Q^2 \leq 2000$ GeV^2. The combined data are compared to QCD predictions in the fixed-flavour-number-scheme (FFNS) and in the general-mass variable-flavour-number-scheme (GM-VFNS) [2].

In FFNS the charm quark is treated as massive and not as a parton in the proton. The number of active flavours is fixed to three, and charm quarks are assumed to be produced only in the hard scattering process via boson-gluon-fusion in leading order. In GM-VFNS charm production is treated as in FFNS in the low Q^2 region where the mass effects are largest, and the charm quark mass is set to zero at high Q^2.

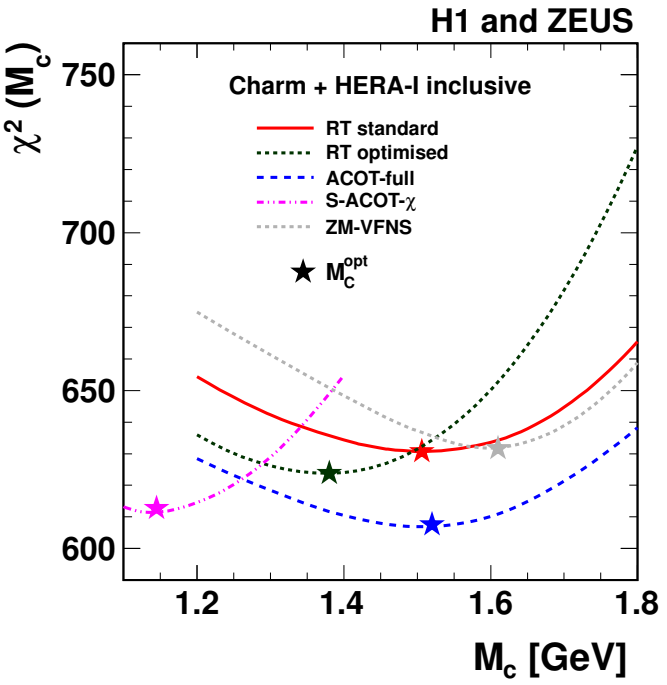

FIG. 10.3 – $\chi^2(M_c)$ for the PDF fit to the combined HERA inclusive DIS and charm measurements. Different heavy flavour schemes used in the fit are presented. The best-fit values $M_c^{\rm opt}$ for each scheme are indicated by the stars.

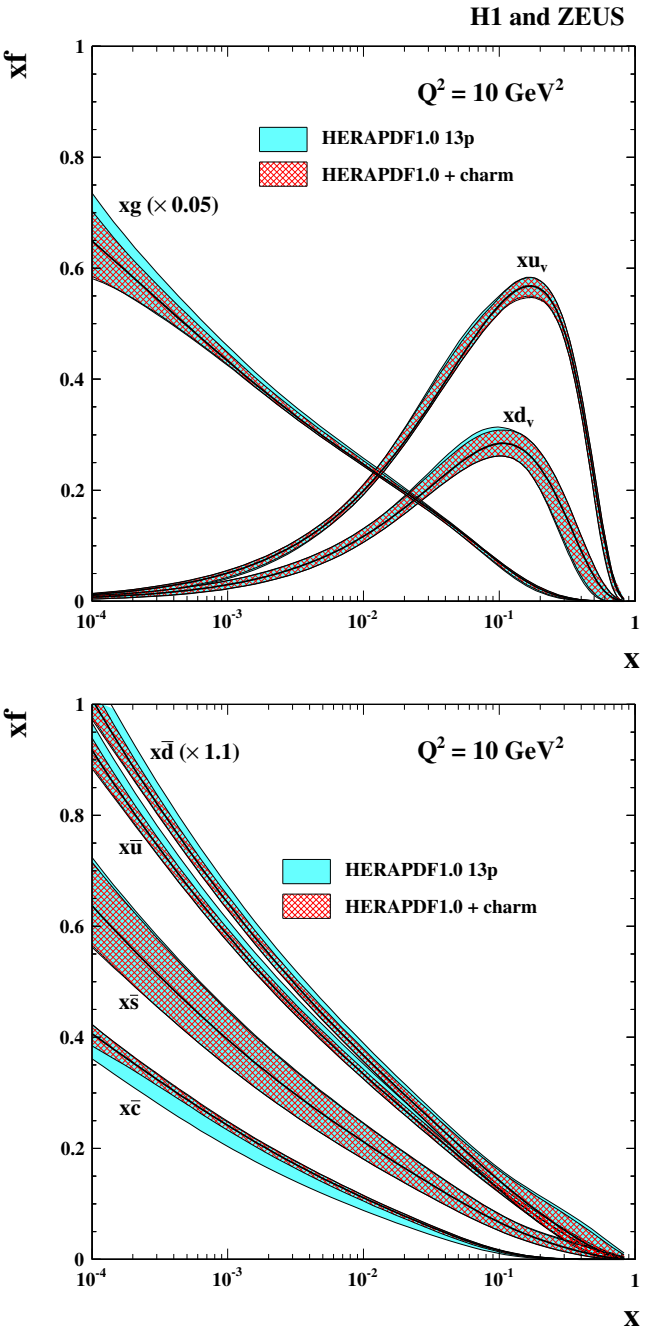

FIG. 10.4 – Parton density functions $x \cdot f(x,Q^2)$ with $f = g, u_v, d_v, \overline{u}, \overline{d}, \overline{s}, \overline{c}$ for (top) valence quarks and gluon and for (bottom) sea anti-quarks obtained from the combined QCD analysis of the inclusive DIS data and $\sigma_{\overline{c}c}$ as a function of x at $Q^2 = 10$ GeV^2. The results of the QCD analysis of the inclusive DIS data only are also shown. For better visibility the gluon distribution function is scaled by 0.05 and the $x\overline{d}$ distribution function by 1.1.

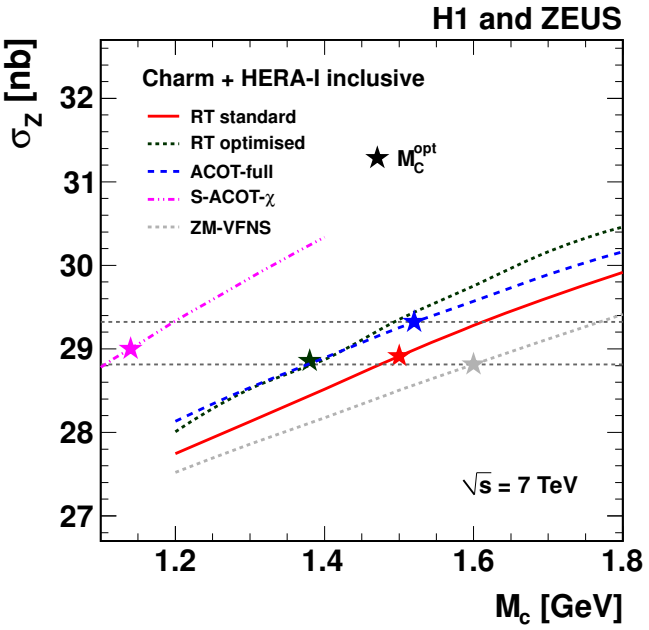

FIG. 10.5 – NLO predictions for the Z production cross sections at the LHC for $\sqrt{s} = 7$ TeV as a function of M_c used in the corresponding PDF fit. Predictions for different implementations of the VFNS are indicated. The predictions obtained with PDFs evaluated with the $M_c^{\rm opt}$ values for each scheme are indicated by the stars. The horizontal dashed lines show the resulting spread of the predictions when choosing $M_c = M_c^{\rm opt}$.

The best description of the data in the whole kinematic range is provided by the most recent NNLO FFNS prediction [4]. Some of the NLO GM-VFNS general-mass predictions significantly underestimate the charm production cross section at low Q^2, which is improved at NNLO. Using the combined charm cross sections together with the combined HERA inclusive DIS data, a NLO QCD analysis was performed based on different VFNS implementations. All schemes are found to describe the data well when treating the charm mass as a free parameter even when the resulting $M_c^{\rm opt}$ may differ considerably (see Fig. 10.3). The use of $M_c^{\rm opt}$ and its uncertainty in the QCD analysis significantly reduces the parton density uncertainties, mainly for the sea quark contributions from charm, down and up quarks (see Fig. 10.4). The QCD analysis was also performed in the FFNS at NLO using the MS running mass definition [4]. The running charm quark mass is determined as $m_c = 1.26 \pm 0.05\,(\text{exp.}) \pm 0.03\,(\text{model}) \pm 0.02\,(\text{param}) \pm 0.02\,(\alpha_s)$ GeV. This value agrees well with the world average based on lattice calculations and on measurements of time-like processes. The PDFs obtained from the corresponding QCD analyses using different M_c are used to predict $W^{\pm}$ and Z production cross-sections at the LHC (see Fig. 10.5). A sizeable spread in the predictions is observed, when the charm mass parameter M_c is varied between 1.2 and 1.8 GeV, or when different schemes are considered at fixed value of M_c. The spread is significantly reduced when the optimal value of M_c is used for each scheme.

10.3 Other subjects

Other subjects which have been addressed in the articles published last year include:

- photoproduction of charm and beauty [5–8];
- diffractive cross sections measured with the forward proton spetrometer [9] and their combination with similar ZEUS-data [10];
- inclusive diffractive contribution to [11] and charged particle spectra from DIS [12].

[1] H1-Collaboration, F.D. Aaron *et al.*, JHEP **09** (2012), 061.

[2] H1- and ZEUS-Collaboration, H. Abramowicz *et al.*, Eur. Phys. J. C **73** (2013), 2311.

[3] H1-Collaboration, F.D. Aaron *et al.*, Eur. Phys. J. C **72** (2012), 2163.

[4] S. Alekhin and S. Moch, Phys. Lett. B **699**, (2011) 345.

[5] H1-Collaboration, F.D. Aaron *et al.*, Eur. Phys. J. C **72** (2012), 1995.

[6] H1-Collaboration, F.D. Aaron *et al.*, Eur. Phys. J. C **72** (2012), 2047.

[7] H1-Collaboration, F.D. Aaron *et al.*, Eur. Phys. J. C **72** (2012), 2148.

[8] H1-Collaboration, C. Alexa *et al.*, *Elastic and Proton Dissociative J/Ψ-Meson Photoproduction at HERA*, submitted to Eur. Phys. J. C (2013), DESY 13 – 058, arXiv:1304.5162 [hep-ex].

[9] H1-Collaboration, F.D. Aaron *et al.*, Eur. Phys. J. C **72** (2012), 1970.

[10] H1- and ZEUS-Collaboration, F.D. Aaron *et al.*, Eur. Phys. J. C **72** (2012), 2175.

[11] H1-Collaboration, F.D. Aaron *et al.*, Eur. Phys. J. C **72** (2012), 2074.

[12] H1-Collaboration, C. Alexa *et al.*, Eur. Phys. J. C **73** (2013), 2406.